

A Higgsploding Theory of Dark Matter

Valentin V. Khoze,^a Joey Reiness,^a Jakub Scholtz^a and Michael Spannowsky^a

^a*Institute for Particle Physics Phenomenology, Department of Physics, Durham University, DH1 3LE, UK*

E-mail: valya.khoze@durham.ac.uk, joey.y.reiness@durham.ac.uk,
jakub.scholtz@durham.ac.uk, michael.spannowsky@durham.ac.uk

ABSTRACT: We show that the Higgspllosion mechanism makes a prediction for the mass and coupling of a WIMP-like minimal scalar dark matter model. In particular the currently favoured minimal value for the Higgspllosion scale, $E_H \sim 25$ TeV, implies a dark matter mass $m_{DM} \sim 1.25$ TeV and a moderate quartic coupling with the Standard Model Higgs field $\lambda_{H,DM} \sim 0.4$. This point in the parameter space is still allowed by all current experimental bounds, including direct detection (XENON), indirect detection (HESS, Fermi, Planck) and collider searches. We have updated the scalar dark matter bounds to reflect the latest results from XENON and HESS experiments. We also comment on vacuum stability and dark matter self-interactions in this model.

Contents

1	Introduction	1
2	A minimal scalar dark matter model	2
2.1	Model	2
2.2	Bare masses, scales and hierarchy	3
2.3	Freeze-Out	4
3	Constraints on the model	5
3.1	Direct detection	5
3.2	Indirect detection: observation of galactic centre by HESS	6
3.3	Other indirect searches	7
3.4	Production at the LHC	8
3.5	Summary of constraints	9
4	Other considerations	10
4.1	DM self-interaction	10
4.2	Vacuum stability and the RG flow of quartic couplings	11
5	Discussion and conclusions	12
5.1	Relaxing assumptions and extending the dark sector	12
5.2	Conclusions	13
	Appendices	15
A	Annihilation cross-sections	15
B	HESS data recast	15
C	More on the RG flow of quartic couplings	16

1 Introduction

It is rather apparent that there is a dark matter (DM) component in our Universe. The earliest evidence comes from the rotation curves of galaxies pioneered by Vera Rubin [1]. There is additional evidence in the power spectrum of the cosmic microwave background (CMB) and large scale structure, as seen most recently by the Planck satellite [2] and the BOSS collaboration [3]. There are geometrical proofs for existence of dark matter [4] inside individual galaxies that do not rely on kinematic information alone. Finally, there

are also colliding clusters of galaxies, such as the Bullet Cluster, that show the need for a non-baryonic matter component in our Universe [5, 6].

Unfortunately, all evidence for dark matter thus far has been of gravitational origin: non-gravitational evidence continues to elude us. Without any such additional evidence, the range of models that both successfully provide the source of dark matter and evade all present constraints is large. The standard DM candidate is a weakly interacting massive particle (WIMP), but there are a plethora of other solutions, such as: axions, fuzzy dark matter, light sterile neutrinos, self-interacting dark matter, dissipative dark matter, atomic dark matter and many more.

In this article we focus on a classic WIMP-like example: a massive scalar whose $\mathcal{O}(1)$ coupling to the Higgs boson naturally generates a correct relic abundance $\Omega_{DM}h^2 = 0.12$ [2]. This scenario has been well explored by many authors [7–11].

Typically, the addition of a light fundamental scalar in a theory introduces hierarchy problems, and so previous scalar dark matter models suffered from inability to predict the preferred mass range for DM. However, in the Higgspllosion scenario [12–14], this large hierarchy problem is greatly reduced by the presence of a new dynamically-generated scale – the Higgspllosion scale. This scale determines corrections to the DM mass. As a result, if the scale is known, we obtain a unique prediction for the mass of minimal scalar dark matter.

Currently the Higgspllosion scale is quantitatively not well known, although existing calculations indicate $E_H \sim 200m_h = 25$ TeV [15] (see also Refs. [16–19] for earlier work). Experimentally, a low Higgspllosion scale can result in striking signatures at high-energy colliders [20]. In this paper we treat the Higgspllosion scale as a free parameter and show that the currently theoretically preferred region for the Higgspllosion scale leads to a dark matter model that is: a) not in tension with any current experimental results, and b) testable in the foreseeable future at direct detection experiments such as LZ and indirect detection experiments such as CTA.

This paper is organized as follows: in Section 2 we describe the model, clarify the scalar mass-Higgspllosion scale relation and enforce the freeze-out constraints. In Section 3 we investigate the viability of such a theory, given both current and projected future constraints from direct detection, indirect detection and production experiments, including XENON and HESS. The strength and relevance of self-interaction and the stability of the vacuum for such a model are discussed in Section 4. Finally, we present our concluding remarks in Section 5.

2 A minimal scalar dark matter model

2.1 Model

In this work, we consider the simplest possible scenario for Higgsploding dark matter: a singlet real scalar, X , with a \mathbb{Z}_2 symmetry [7–9]. The dark and Standard Model sectors communicate via a Higgs-portal coupling, λ_{HX} ,

$$\mathcal{L} = \mathcal{L}_{SM} + \frac{1}{2}\partial_\mu X \partial^\mu X - \frac{1}{2}m_{X,0}^2 X^2 - \frac{\lambda_X}{4!}X^4 - \frac{\lambda_{HX}}{2}X^2 \left(H^\dagger H\right), \quad (2.1)$$

with,

$$\mathcal{L}_{SM} \supset \mu_0^2 H^\dagger H - \lambda_H (H^\dagger H)^2. \quad (2.2)$$

For now, we make the assumption that $\lambda_X \ll \lambda_{HX}$. In Section 4.2, we confirm this is a safe assumption, despite the renormalization group (RG) flow. We also assume that the bare mass is small, such that the renormalized mass of the dark scalar is dominated by the quadratically-divergent contribution from loops of Higgs particle,

$$m_X^2 = m_{X,0}^2 + \delta m_X^2 \approx \delta m_X^2 \approx \frac{\lambda_{HX} \Lambda_{UV}^2}{16\pi^2}, \quad (2.3)$$

where Λ_{UV} is the UV cut-off of the theory. In a Higgsploding theory, as discussed in [12–15], this cut-off becomes physical. Above a certain virtuality, called the Higgspllosion scale E_H , the Higgs bosons are expected to decay exponentially into a large number of soft quanta, a phenomenon dubbed Higgspllosion. The imaginary part of the self-energy for the Higgs particle grows exponentially with the virtuality of the propagator and the Higgs propagator effectively vanishes above E_H . This has the consequence of cutting off integrals over Higgs four-momenta, k^μ , at $k^\mu k_\mu = E_H^2$. Hence, in the regime described, we expect a dark scalar mass of order

$$m_X^2 \approx \lambda_{HX} \frac{E_H^2}{16\pi^2}. \quad (2.4)$$

If the Higgspllosion scale is known, this relation greatly restricts the parameter space available, and uniquely determines the dark matter mass when combined with the freeze-out condition, as we will show in Section 2.3.

As we will see, the region of parameter space corresponding to large mass and portal coupling remains unbounded for our model. As a result, we must choose a maximal coupling strength that we consider perturbatively under control. In this work, we choose a somewhat conservative value, $\lambda_X, \lambda_{HX} \leq \sqrt{8\pi} \simeq 5$ [21].

2.2 Bare masses, scales and hierarchy

Typically, in order to arrive at the IR spectrum we observe for the SM, we must fine-tune the Higgs bare mass in the UV – this is the Hierarchy problem. This problem persists in the presence of Higgspllosion, but is significantly reduced. In order to achieve the observed Higgs mass, the bare mass must now instead satisfy,

$$\mu_0^2 = -\frac{\lambda_H}{2} v_{EW}^2 - E_H^2 \left(\frac{\lambda_H}{4\pi^2} + \frac{\lambda_{HX}}{16\pi^2} - \frac{N_c y_t^2}{8\pi^2} + \dots \right), \quad (2.5)$$

where the first term is the Higgs doublet mass required to break the electroweak symmetry and the remaining terms are self-energy corrections, with N_c quark colours. In the Higgsploding regime, we expect the scale of all of these contributions to be proportional to E_H^2 : if any particle reaches virtuality of order E_H^2 , its self-energy quickly suppresses its propagator. As a result, the Higgs mass¹ is fine-tuned to the extent of $\sqrt{\lambda_H} v_{EW} / E_H \sim 10^{-2}$, which is a vast improvement when compared to the usual fine-tuning of order $m_h / m_{GUT} \sim 10^{-14}$.

Given that X is also a scalar, one might expect it to exhibit its own Higgspllosion-like behaviour, which we dub “Xpllosion”². Indeed, in the limit $\lambda_{HX} \rightarrow 0$, the dark sector

¹The top quark contribution is also reduced by Higgspllosion, we refer the reader to references [12–15]

²This “pun” being the sole reason for our particle naming scheme.

decouples from the SM sector and one could expect the amplitude for the process

$$X \rightarrow nX, \quad (2.6)$$

to grow exponentially at some Xplosion scale, $E_X \propto f(8\pi/\lambda_X)m_X$, where $f(8\pi/\lambda_X)$ becomes infinite in the limit $\lambda_X \rightarrow 0$. In the symmetric phase of the theory, the processes (2.6) most likely remains negligible. It is only in the broken phase, i.e. for the scalar X model with the spontaneously broken \mathbb{Z}_2 symmetry, that the calculations of quantum effects summarised in [14, 15] would lead to Xplosion. However, in the \mathbb{Z}_2 symmetric case relevant here, where X is the scalar DM candidate, quantum effects are known to exponentially suppress the effect of Xplosion seen at the classical level. Furthermore, we have assumed that $\lambda_{HX} \neq 0$ and $m_X \gg m_h$, so the Higgsplosion process,

$$X \rightarrow X + nh, \quad (2.7)$$

is allowed at far lower virtualities of order $m_X^2 + E_H^2 \ll E_X^2$. Even if Xplosion (2.6) was possible, Higgsplosion (2.7) ultimately determines the UV behaviour of X .

In our scenario we set the bare mass of X to be relatively small,

$$-\frac{\lambda_{HX}}{16\pi^2}E_H^2 \lesssim m_{X,0}^2 \lesssim \frac{\lambda_{HX}}{16\pi^2}E_H^2, \quad (2.8)$$

so that the self-energy contribution is dominant. In that sense, the mass of X is natural.

2.3 Freeze-Out

In this subsection, we follow treatment of freeze out calculations as summarised in [8, 22]. An important quantity in the calculations to follow is the thermally-averaged dark matter annihilation cross-section $\langle \sigma_{ann} v_{rel} \rangle \equiv \langle \sigma v \rangle$. The contributions to this cross-section for different annihilation modes were calculated in [7]. We include the exact results in Appendix A.

In the regime $m_X \gg v$, where v is the Standard Model Higgs vacuum expectation value, the annihilation cross-section is dominated by the hh , $W_L^+ W_L^-$ and $Z_L^0 Z_L^0$ modes. This is not surprising: these modes are the four degrees of freedom of the Higgs doublet that directly couple to X through the $\lambda_{HX} X^2 H^\dagger H$ operator. In the regime $m_X^2 \gg \{v^2, m_h^2, m_W^2, m_Z^2\}$ the annihilation cross-section simplifies to:

$$\langle \sigma v \rangle \approx \frac{\lambda_{HX}^2}{16\pi m_X^2}. \quad (2.9)$$

We will see that $m_X \lesssim v$ leads to values for the Higgsplosion scale that are too low, and so we can safely ignore the low-mass regime entirely. As a result, we will use the approximation of Eq. 2.9 throughout this paper.

The relic density of dark matter today is constrained by the Planck satellite [2] to $\Omega_{DM} h^2 = 0.12$. Our prediction for the present day density of X particles is [8, 22, 23]:

$$\Omega_X h^2 = \left[\frac{8\pi G g_*(m_X/x_f)}{45} \right]^{1/2} \frac{4\pi^2 G x_f T_0^3}{45 \langle \sigma v \rangle H_{100}^2}, \quad (2.10)$$

where $g_*(m_X/fx_f)$ denotes the number of degrees of freedom in equilibrium at annihilation, T_0 is the current temperature, $H_{100} = 100 \text{ km s}^{-1} \text{ Mpc}^{-1}$, and G is the Newton's constant. We determine the inverse freeze-out temperature, $x_f = m_X/T_F$, by solving the implicit equation,

$$x_f \sim \ln \left[\sqrt{\frac{45}{4\pi^5}} \frac{1}{\sqrt{g_*}} \frac{m}{\sqrt{8\pi G}} \langle \sigma v \rangle \right] - \frac{1}{2} \ln^2 \left[\sqrt{\frac{45}{4\pi^5}} \frac{1}{\sqrt{g_*}} \frac{m}{\sqrt{8\pi G}} \langle \sigma v \rangle \right]. \quad (2.11)$$

Solving the above equation for a perturbative range of λ_{HX} yields the usual x_f values in the range 20–30. The freeze-out condition in Eq. (2.10) gives a relationship between λ_{HX} and m_X :

$$\lambda_{\text{HX}} = 0.30 \left(\frac{x_f}{20} \right)^{1/2} \left(\frac{\Omega_X h^2}{0.12} \right)^{1/2} \left(\frac{m_X}{1 \text{ TeV}} \right). \quad (2.12)$$

The combination of imposing the Higgsploding scenario, keeping λ_{HX} perturbative and demanding the correct relic density greatly limits the allowed DM mass range.

Recall that we have not fixed the Higgspllosion scale E_H . Instead, in the regime considered, it is uniquely specified by the values of λ_{HX} and m_X as argued in Section 2.1. It is worth noting that the parameter space would be larger if we relaxed the assumption that $\lambda_X \ll \lambda_{\text{HX}}$, or allowed for a fine-tuning between the bare mass term and the λ_{HX} loop contribution.

Finally, we note that $\langle \sigma v \rangle$ is the cross-section at the time of freeze out, $T_f = m_X/x_f \sim 0.1 m_X$, when the X species was relativistic. Therefore, the Sommerfeld enhancement [9, 24] is negligible.

3 Constraints on the model

3.1 Direct detection

We are now in a position to calculate the cross-sections expected in direct detection experiments, using the values of m_X and λ_{HX} that are allowed by the relic density. The DM-nucleon cross-section is given by [10] and adapted here for the large mass limit, $m_X > m_N$):

$$\sigma_{SI} = \frac{\lambda_{\text{HX}}^2 f_N^2}{4\pi} \frac{m_N^2 m_X^2}{(m_N + m_X)^2} \frac{m_N^2}{m_h^4 m_X^2} \sim \frac{\lambda_{\text{HX}}^2 f_N^2}{4\pi} \frac{m_N^4}{m_h^4 m_X^2}, \quad (3.1)$$

where m_N is the mass of a nucleon and $f_N \sim 0.3$ is an effective Higgs-nucleon-nucleon coupling.

Specifying a DM mass uniquely determines λ_{HX} and E_H for a Planck relic density, and so we can see how the elastic cross-section, σ_{SI} , varies with DM mass, m_X . This dependence is plotted in Fig. 1, with the Higgspllosion scale shown on the top axis, and the associated quartic coupling, λ_{HX} , indicated for a selection of points on the line. Present and projected constraints from LUX [25], Xenon-1T [26] and LZ [27] are shown for reference. We see that current constraints exclude DM masses below $\sim 0.7 \text{ TeV}$, with future searches such as LZ probing the remaining perturbative parameter space. Note that both σ_{SI} and

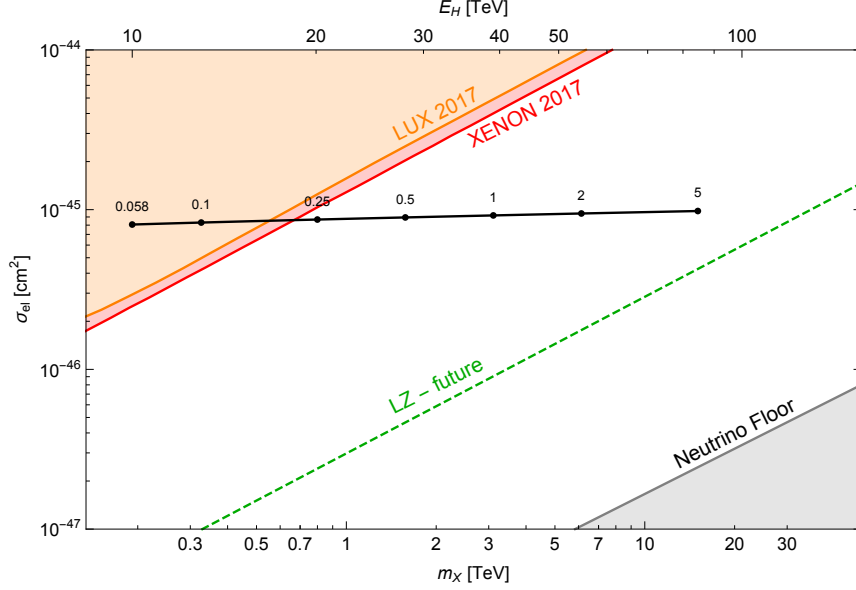


Figure 1: Constraints on possible real singlet DM masses from present and projected future direct detection experiments. Demanding Planck relic density confines the possible values to the black line, with values of portal couplings λ_{HX} indicated for a selection of points on said line. The line terminates at the onset of non-perturbative behaviour at $\lambda_{HX} = 5$. The Higgspllosion scale E_H required to attain a given mass is shown on the top axis. We see that masses below ~ 0.7 TeV are excluded by current experiments. The future experiment, LZ, is predicted to probe the remaining perturbative mass range [27].

$\langle\sigma v\rangle$ are proportional to λ_{HX}^2/m_X^2 . Hence, maintaining the correct relic density keeps σ_{SI} constant, up to the logarithmic corrections from x_f .

We now shift our focus to indirect detection.

3.2 Indirect detection: observation of galactic centre by HESS

In this section we compare the constraints on annihilation cross-section derived from ten years of observations of the inner 300 pc of the galactic centre region by the HESS experiment [28] with cross-section values predicted for our DM scalar. This involves looking at the expected photon spectrum for the processes $XX \rightarrow \{hh, W^+W^-, \tau\tau\} \rightarrow \gamma\gamma$, which we obtain using Cirelli’s data and associated Mathematica package [29].

The HESS data is presented in [28] as constraints on $\langle\sigma v\rangle$ for $XX \rightarrow \bar{J}J$, where $J \in \{W, \tau\}$. Unfortunately, our scalars annihilate into hh , $W_L W_L$ and $Z_L Z_L$. However, the supplied information is sufficient for a conservative bound. The rationale used in our recast is that the number of photons predicted in any bin should not exceed the number of observed photons in this bin. The conservative upper bound can be related to the constraints on the WW and $\tau\tau$ channels. For a more in-depth explanation of the procedure,

see Appendix B. We find that,

$$\langle\sigma v\rangle(XX \rightarrow \text{SM}) \leq \min_{E \in [10\text{GeV}, 30\text{TeV}]} \left[\frac{4 \max \left(\sigma_{WW} \frac{dn_{WW}}{dE}, \sigma_{\tau\tau} \frac{dn_{\tau\tau}}{dE} \right)}{\left(\frac{dn_{hh}}{dE} + 2 \frac{dn_{LL}}{dE} + \frac{dn_{ZZ}}{dE} \right)} \right], \quad (3.2)$$

where σ_{WW} and $\sigma_{\tau\tau}$ are the HESS constraints on DM annihilating dominantly into WW and $\tau\tau$ channels, and dn_{ii}/dE are the spectra of photons from annihilations $XX \rightarrow ii$. Since the annihilations are non-relativistic, the total cross-section computed at leading order should be corrected to account for a potentially large effect due to multiple t -channel exchanges of the light Higgs bosons between the non-relativistic X scalars, $m_X \gg m_h$. This gives rise to the multiplicative Sommerfeld enhancement factor \mathcal{S} for the total cross-section. However, the effective coupling for $XX \rightarrow XX$ scattering through the t -channel Higgs is not $\alpha \equiv \lambda_X^2/4\pi$, but instead a much smaller,

$$\alpha \equiv \left(\frac{v_{EW}}{m_X} \right)^2 \frac{\lambda_X^2}{4\pi}. \quad (3.3)$$

This can be obtained directly by extracting the pre-factor of the Yukawa potential obtained by matching the amplitude for the process $XX \rightarrow XX$. As a result, when we use the analytic approximation (obtained from the Hulthén potential) for \mathcal{S} given in [24],

$$\mathcal{S} = \frac{\pi}{\epsilon_v} \frac{\sinh \left(\frac{2\pi\epsilon_v}{\pi^2\epsilon_h/6} \right)}{\cosh \left(\frac{2\pi\epsilon_v}{\pi^2\epsilon_h/6} \right) - \cos \left(2\pi \sqrt{\frac{1}{\pi^2\epsilon_h/6} - \frac{\epsilon_v^2}{(\pi^2\epsilon_h/6)^2}} \right)}, \quad (3.4)$$

we need to choose $\epsilon_v \equiv 4\pi v/\lambda_{HX}^2(m_X/v_{EW})^2$ and $\epsilon_h \equiv 4\pi m_X m_h/(v_{EW}^2 \lambda_{HX}^2)$ with velocity $v = 10^{-4}c \sim 30\text{km/s}$. For this reason, we find a very minimal Sommerfeld enhancement for the range of DM masses considered, despite the non-relativistic velocity. Finally, we also find that the enhancement factor in the relevant mass range is largely unchanged by up to order-of-magnitude changes in the velocity v .

Both the original and recast HESS results are shown in Fig. 2, which will be discussed in Section 3.5, once all potentially competitive detection methods have been addressed.

3.3 Other indirect searches

Ultimately, we will see that HESS provides the strongest current indirect detection constraints on our model. However, it is worth discussing other current searches, as well as projected future constraints:

- The Fermi Large Area Telescope records gamma-ray emission from dwarf spheroidal galaxies, which can be used to derive constraints on the annihilation cross-section, $\langle\sigma v\rangle$, [10, 30–33].
- The Planck satellite measures CMB anisotropy, which once again can be used to calculate constraints on the annihilation cross-section [34, 35].

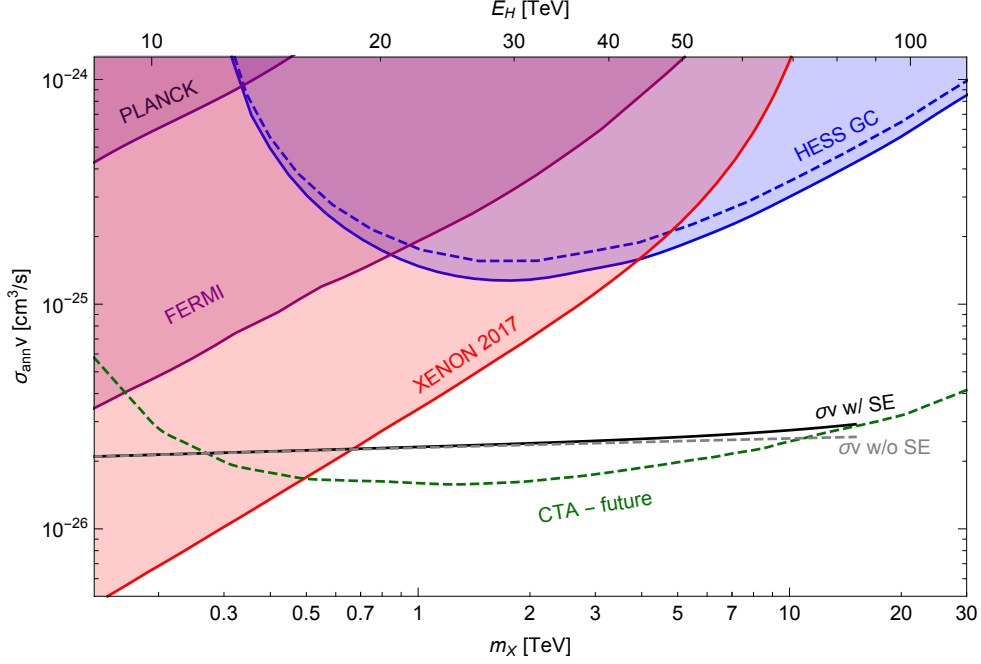


Figure 2: Predicted theoretical annihilation cross-sections $\langle\sigma v\rangle$ for $XX \rightarrow \gamma\gamma$ in the galactic centre (GC) compared to indirect detection constraints from PLANCK, FERMI and HESS data, as well as the direct detection constraint from XENON 2017, reinterpreted in terms of $\langle\sigma v\rangle$. Shaded regions are excluded. The solid blue line indicates the recast HESS constraint which is conservative and the dashed blue line shows the constraint on pure WW decay channel. The real constraint will lie somewhere between the two, but fortunately the difference is minimal. The predicted cross-section is shown with and without Sommerfeld enhancement, up to the DM mass corresponding to a non-perturbative portal coupling, $\lambda_{\text{HX}} = 5$. DM particles in the GC are expected to be non-relativistic, so enhancement considerations are necessary. We see that for the DM masses allowed by a perturbative coupling, the enhancement is minimal. The projected future constraint from CTA is shown to probe the remaining perturbative parameter space.

- The Cherenkov Telescope Array (CTA) is a future ground-based gamma-ray observatory, which among other things, will observe the galactic centre. We use the projected constraints computed by [36].

The constraints from the above experiments on the annihilation cross-section are shown along with the HESS and XENON constraints in Fig. 2, which will be discussed in Section 3.5.

3.4 Production at the LHC

In general, this class of models is very hard to discover at colliders: full production cross-section at the LHC is suppressed for three reasons: 1) Since the final state XX is invisible we need to recoil against additional radiation, 2) the XX state is only accessible through

weak couplings in the VBF scenario or through an off-shell Higgs, 3) the mass of X is large enough to pose kinematic suppression. As a result, according to [37], at a 100 TeV collider, even with 30ab^{-1} , we become 1σ sensitive to $\lambda_{\text{HX}} \sim 1$ for $m_X \lesssim 200$ GeV. This is well outside of the region we consider in this work.

3.5 Summary of constraints

The constraints imposed by the various direct and indirect searches described in the previous sections on annihilation cross-section are compared to the theoretical prediction (with and without Sommerfeld Enhancement) in Fig. 2. In order to include the direct detection constraints from XENON 2017 on this plot, we have re-interpreted the XENON 2017 exclusion contour for σ_{SI} in terms of the corresponding annihilation cross-sections, $\langle\sigma v\rangle$, using Eq. (3.1).

We see that, ultimately, HESS and XENON 2017 provide the strongest current exclusions. The Planck and Fermi results are thus omitted from later plots in the interest of clarity. The dashed blue line indicates the original WW HESS data, with the solid blue line showing the conservative recast. The real constraint will lie somewhere between the two, but fortunately the difference is minimal.

The region of interest is shown in $(m_X, \lambda_{\text{HX}})$ space in Fig. 3. The numbered points on the black critical density line indicate the Higgs-plosion scale required for that mass and coupling in TeV. We thus find ourselves with the following ranges (which are of course coupled):

$$\begin{aligned} 0.7 \text{ TeV} &\lesssim m_X &&\lesssim 15 \text{ TeV} \\ 19 \text{ TeV} &\lesssim E_H &&\lesssim 85 \text{ TeV} \\ 0.2 &\lesssim \lambda_{\text{HX}} &&\lesssim 5 \end{aligned} \tag{3.5}$$

The upper bound to this range, at least currently, comes from the requirement of a perturbative coupling. The point at which the coupling becomes non-perturbative is ill-defined and somewhat subjective: as such, so is the upper bound. We choose a maximum coupling of $\lambda_{\text{HX}} = \sqrt{8\pi} \simeq 5$. The lower bound is given by the XENON 2017 direct detection constraints and is far-better defined.

Conveniently, this range is accessible by detectors currently in development, such as CTA and LZ [27, 36]. The model considered in this work is of course very minimal, but it is interesting that it is testable in the next decade. The dashed grey line indicates the masses and couplings required for correct relic density in the case that X is a complex scalar. We see that this scenario gives a similar but slightly stricter range.

The bounds in Fig. 3 were calculated under the assumption that the scalar DM was the sole contributor to the correct relic density, $\Omega h^2 = 0.12$. However, in the interest of completeness, Fig. 4 shows the same bounds but derived using a relic density dictated by m_X and λ_{HX} as independent parameters. Essentially, the direct detection limits are rescaled by α and indirect by α^2 , where $\alpha(m_X, \lambda_{\text{HX}}) = \Omega h^2(m_X, \lambda_{\text{HX}})/0.12$. Unsurprisingly, the XENON and HESS curves still cross the black line of correct relic values at the same points, as this is where $\alpha = 1$. Once again, LZ and CTA will be able to comfortably probe the entire parameter space predicted in our model.

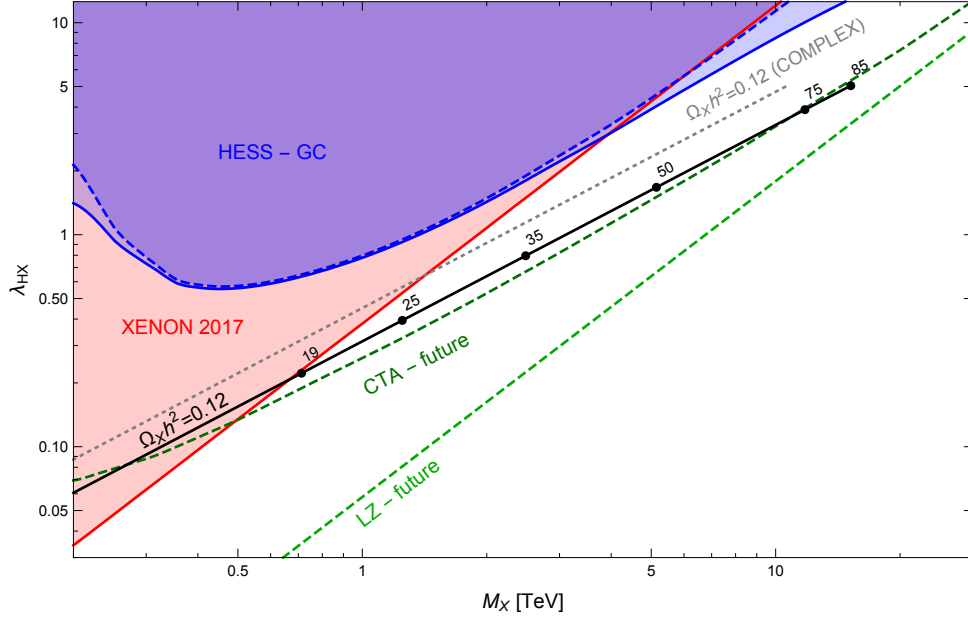


Figure 3: Constraints from direct and indirect detection, in mass-coupling space. Demanding correct relic density confines the possible values to the black line, with numbered points indicating the required Higgspllosion scale E_H in TeV. We end our line at a coupling of $\lambda_{HX} = 5$, which we consider non-perturbative. The grey dashed line traces the same observed value of the relic density but for the case of a complex scalar. The HESS constraints are shown with (solid blue) and without (dashed blue) Sommerfeld enhancement. We see a small effect in the regions of higher couplings. For X real and perturbative coupling, we are left with a range of possible DM masses and the corresponding E_H values in the range $19 \text{ TeV} \lesssim E_H \lesssim 85 \text{ TeV}$, that are experimentally viable. As in earlier plots, the projected future constraints from LZ and CTA probe the entire remaining parameter space.

4 Other considerations

4.1 DM self-interaction

In this section we assess the extent of DM self-interaction in our model. Recent work has suggested that strong DM self-interactions can change inner-halo structure and give better agreement with short-scale observations than regular cold dark matter (CDM) models. To solve these small-scale discrepancies, such as the “core-cusp” problem, we require a self interaction cross-section per mass of $\sigma(XX \rightarrow XX)/m_X \sim 1 \text{ cm}^2 \text{ g}^{-1}$ [38, 39].

Self scattering is determined by two processes: $XX \rightarrow XX$, with amplitude proportional to λ_X , and $XX \rightarrow h^* \rightarrow XX$, with amplitude proportional to $\lambda_{HX}^2 v^2 / m_h^2$. Since we require $\lambda_X \ll \lambda_{HX}$ in our model, the Higgs exchange process dominates the amplitude. Summing the contributions from the s, t and u channels and calculating the cross-section yields a non-trivial expression. However, for $m_h \ll m_X$ and under the assumption that that the initial and final X particles are non-relativistic, $v \ll 1$, we find the leading order

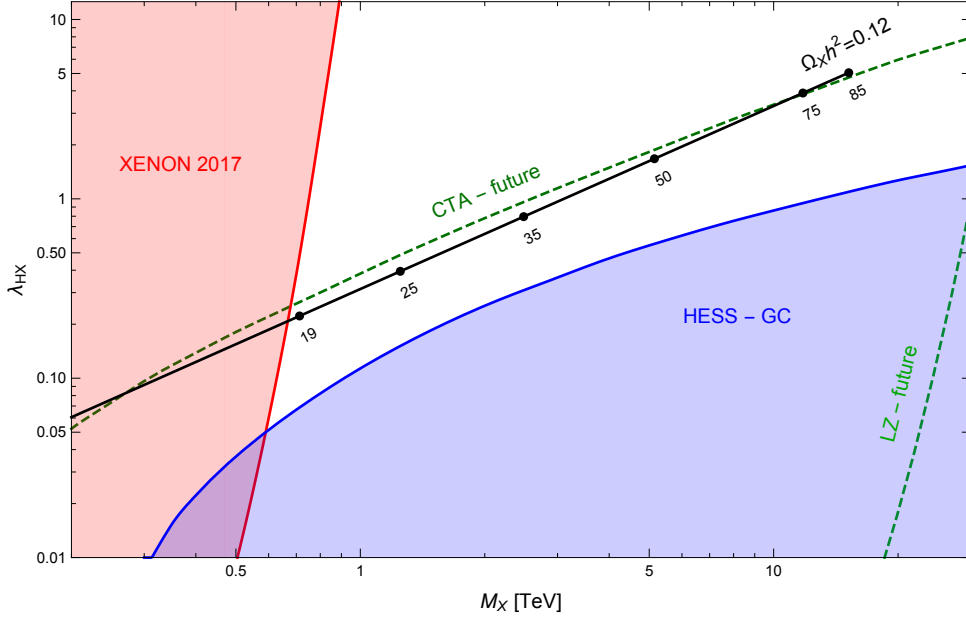


Figure 4: Constraints from direct and indirect detection, in mass-coupling space. However, constraints are now derived without assuming correct relic density: i.e. given a relic density dictated by the (m_X, λ_{HX}) values as free independent parameters. As in Fig. 3, demanding correct relic density confines the possible values to the black line, with numbered points indicating the required Higgspllosion scale in TeV. We once again end our line at a coupling of $\lambda_{HX} = 5$, which is considered non-perturbative. Note that for this plot, the projected exclusion zone for CTA is below its line, whereas the projected exclusion zone for LZ is above.

term,

$$\sigma(XX \rightarrow XX) = \frac{v_{EW}^4 \lambda_{HX}^4}{16 m_h^4 m_X^2} + \mathcal{O}(v^2, m_h^{-2}), \quad (4.1)$$

where v is the velocity, whereas v_{EW} is the Higgs VEV as before. This corresponds to a cross-section per mass of order

$$\begin{aligned} \frac{\sigma(XX \rightarrow XX)}{m_X} &\approx \lambda_{HX}^4 \left(\frac{m_X}{1 \text{ TeV}} \right)^{-3} (2.1 \times 10^{-15} \text{ cm}^2 \text{ g}^{-1}) \\ &\approx 10^{-18} \text{ cm}^2 \text{ g}^{-1} \left(\frac{x_f}{20} \right)^2 \left(\frac{\Omega_X h^2}{0.12} \right)^2 \left(\frac{m_X}{1 \text{ TeV}} \right). \end{aligned} \quad (4.2)$$

As a result, even with large Sommerfeld enhancement, we do not expect to see any significant self-interaction for this dark matter model.

4.2 Vacuum stability and the RG flow of quartic couplings

In this section we will show that the vacuum of our model is stable at the tree level and that this property is unchanged by renormalisation group (RG) flow. The scalar potential

in our theory is given by,

$$V(A, B) = -\mu_0^2 A + \frac{1}{2} m_{X,0}^2 B + \lambda_H A^2 + \frac{\lambda_X}{4!} B^2 + \frac{\lambda_{HX}}{2} AB, \quad (4.3)$$

where $A = H^\dagger H > 0$ and $B = X^2 > 0$. Vacuum stability is achieved if either of the following criteria is satisfied:

$$\begin{aligned} \text{if } \lambda_{HX} < 0 : \quad & \lambda_H, \lambda_X > 0 \quad \text{and} \quad \lambda_H \lambda_X > \frac{3}{2} \lambda_{HX}^2, \\ \text{if } \lambda_{HX} > 0 : \quad & \lambda_H, \lambda_X > 0. \end{aligned} \quad (4.4)$$

The case of negative λ_{HX} is in tension with our earlier assumption of $\lambda_{HX} \gg \lambda_X$, because negative λ_{HX} implies $\lambda_H \lambda_X > \frac{3}{2} \lambda_{HX}^2$. However, if all three couplings are positive, the vacuum is stable even for $\lambda_{HX} \gg \lambda_X$. In both scenarios, the vacuum is most easily destabilised if λ_X runs to a negative value.

Since we require $\lambda_X \ll \lambda_{HX} \sim 1$, a small change to λ_X due to RG flow can change the sign of λ_X with catastrophic consequences. We require small λ_X at RG scale $\mu = E_H$, in order to avoid additional contribution to m_X . Above E_H the RG flow is frozen due to the Higgsplosion of the self-energy leading to the Higgsplosion of full propagators [12–14]. Hence, we need only worry about the small region between m_X and E_H . In this region, the approximate change to λ_X , $\delta\lambda_X$, is simply,

$$\delta\lambda_X \sim \beta_{\lambda_X} \log\left(\frac{m_X}{E_H}\right) \sim -\frac{3}{16\pi^2} \lambda_{HX}^2 \log\left(\frac{4\pi}{\sqrt{\lambda_{HX}}}\right), \quad (4.5)$$

where β_{λ_X} is the beta function for the quartic X coupling (for full expressions see Appendix C). As long as $\lambda_X(E_H) > |\delta\lambda_X|$, then the vacuum is stable. As a result we require:

$$\lambda_X \gtrsim \frac{3\lambda_{HX}^2}{16\pi^2} \log\left(\frac{4\pi}{\sqrt{\lambda_{HX}}}\right). \quad (4.6)$$

For the two extremal allowed values of $\lambda_{HX} = 0.2$ and $\lambda_{HX} = 5$, this corresponds to $\lambda_X \gtrsim 2.5 \times 10^{-3}$ and $\lambda_X \gtrsim 0.82$ respectively. As a result, it is always possible to achieve at least $\lambda_X/\lambda_{HX} \lesssim 0.17$, and so our assumption, $\lambda_X \ll \lambda_{HX}$, is safe (particularly for lower DM masses). We perform a more accurate analysis with the full coupled evolution of all three couplings $\{\lambda_X, \lambda_{HX}, \lambda_H\}$ in Appendix C. The conclusions remain essentially the same: we can achieve vacuum stability at all scales, while maintaining the core assumption of this work, $\lambda_X \ll \lambda_{HX}$.

5 Discussion and conclusions

5.1 Relaxing assumptions and extending the dark sector

In this paper we have made the following assumptions:

1. There is no fine-tuning in the mass of X . Furthermore, the radiative correction to the mass of X is determined by corrections from the Higgs particle.

2. X is the sole component of a dark sector.

If we were to relax these assumptions, the constraints on this model would be weakened. Consider the following examples:

1. Breaking the first assumption has simple consequences. Requiring the correct relic density still fixes a relationship between λ_{HX} and m_X . However, allowing for additional contributions, μ_X^2 , to the DM mass relaxes the relationship between λ_{HX} , m_X and E_{H} ,

$$m_X^2 = \mu_X^2 + \lambda_{\text{HX}} \frac{E_{\text{H}}^2}{16\pi^2}. \quad (5.1)$$

As a result, for negative μ_X^2 we can obtain the same combination of λ_{HX} and m_X for a higher value of E_{H} . From the point of view of physics below the Higgsplosion scale, nothing is influenced by this fine-tuning.

2. Breaking the second assumption can be done in many ways and the phenomenological implications are just as varied. For example, we can introduce another species that X can freeze-out into. Consequently, the annihilation cross-section for XX may become independent of λ_{HX} and completely ruin the predictive power of this model: we can set λ_{HX} arbitrarily small and make X invisible while maintaining the correct relic density. For another example of breaking the second assumption, we refer the reader to [40].

Though all these changes to our model are reasonable, they do lead to less predictive and more complicated scenarios. We therefore refrain from exploring such extensions.

5.2 Conclusions

In this paper we have shown that the Higgsplosion mechanism results in a definite prediction for mass of a real scalar dark matter candidate, as well as a definite prediction of its coupling to the Standard Model fields. In particular, the lowest value for the Higgsplosion scale theoretically preferred, i.e. $E_{\text{H}} \sim 25$ TeV, implies a dark matter mass of $m_X \sim 1.25$ TeV and a Higgs portal coupling $\lambda_{\text{HX}} \sim 0.4$, which remains safe from all current constraints.

In order to check the viability of this scenario, we have updated the direct detection constraints on scalar dark matter models for the newest dataset from the XENON experiment, and have recast recent HESS indirect detection results.

This particular model can be probed by future indirect detection experiments such as CTA, and as well as by the direct detection experiment LZ, both of which should start collecting data within the next decade. As a result, we have presented a definite prediction for a model of dark matter that can be, in its present form, discovered in the foreseeable future. It is possible to relax some of the (fairly strict) assumptions to relax bounds on this model, at the cost of loss of predictivity. We invite anyone interested to do so.

Acknowledgements

We would like to thank Mikael Chala, Richard Ruiz and Matthew Kirk for helpful discussions.

Appendices

A Annihilation cross-sections

Below are the cross-sections for annihilation modes as calculated in [7]:

$$\begin{aligned}
\langle\sigma_{hhv}\rangle &= \frac{\lambda_{\text{HX}}^2}{64\pi m_X^2} \left(1 - \frac{m_h^2}{m_X^2}\right)^{1/2} \xrightarrow{m_X^2 \gg m_h^2} \frac{\lambda_{\text{HX}}^2}{64\pi m_X^2}, \\
\langle\sigma_{WWv}\rangle &= \frac{\lambda_{\text{HX}}^2 m_W^4 [2 + (1 - 2m_X^2/m_W^2)^2]}{8\pi m_X^2 [(4m_X^2 - m_h^2)^2 + m_h^2 \Gamma_h^2]} \left(1 - \frac{m_W^2}{m_X^2}\right)^{1/2} \xrightarrow{m_X^2 \gg m_h^2, m_W^2} \frac{\lambda_{\text{HX}}^2}{32\pi m_X^2}, \\
\langle\sigma_{ZZv}\rangle &= \frac{\lambda_{\text{HX}}^2 m_Z^4 [2 + (1 - 2m_X^2/m_Z^2)^2]}{16\pi m_X^2 [(4m_X^2 - m_h^2)^2 + m_h^2 \Gamma_h^2]} \left(1 - \frac{m_Z^2}{m_X^2}\right)^{1/2} \xrightarrow{m_X^2 \gg m_h^2, m_Z^2} \frac{\lambda_{\text{HX}}^2}{64\pi m_X^2}, \\
\langle\sigma_{ffv}\rangle &= \frac{\lambda_{\text{HX}}^2 m_f^2}{4\pi [(4m_X^2 - m_h^2)^2 + m_h^2 \Gamma_h^2]} \left(1 - \frac{m_f^2}{m_X^2}\right)^{3/2} \xrightarrow{m_X^2 \gg m_h^2, m_f^2} \frac{\lambda_{\text{HX}}^2}{64\pi m_X^2} \frac{m_f^2}{m_X^2}.
\end{aligned} \tag{A.1}$$

We see that in the limit $m_X^2 \gg m_h^2, m_W^2, m_Z^2, m_f^2$, the total annihilation cross-section is:

$$\langle\sigma v\rangle = \frac{\lambda_{\text{HX}}^2}{16\pi m_X^2} + \mathcal{O}\left(\frac{m_h^2}{m_X^2}, \frac{m_W^2}{m_X^2}, \frac{m_Z^2}{m_X^2}, \frac{m_f^2}{m_X^2}\right) \tag{A.2}$$

B HESS data recast

The HESS instrument has measured the high energy photon spectrum over the last 10 years (254 hours of observation) [28]. Unfortunately, there are only two dark matter annihilation channels whose cross-sections have been officially constrained by the HESS data: $XX \rightarrow W^+W^-$ and $XX \rightarrow \tau^+\tau^-$. We will reinterpret these results in order to derive a conservative constraint on a combination $XX \rightarrow H^\dagger H$, which is a weighted combination of three channels $XX \rightarrow hh$, $XX \rightarrow W_L^+W_L^-$ and $XX \rightarrow Z_L Z_L$.

First we define several variables: let \mathcal{L} be the line of sight integral,

$$\mathcal{L} = \int n^2 dl, \tag{B.1}$$

where n is the dark matter density, such that $\mathcal{L}\langle\sigma v\rangle$ gives the rate of dark matter particle annihilation along the line of sight. Note that \mathcal{L} only depends on the dark matter density along the line of sight and so it is independent of the annihilation channel we are constraining.

Furthermore, we define the spectral density of photons from a single annihilation of two dark matter particles into a final state J as dn_J/dE . For example, the spectrum of photons from the process $XX \rightarrow W_L W_L$ is denoted by $dn_{W_L W_L}/dE$. Note that the integral,

$$N_\gamma = \int_{E_0}^{\infty} \frac{dn_J}{dE} dE = \langle N_\gamma(E > E_0) \rangle, \tag{B.2}$$

is the average number of photons with energy larger than E_0 from a single annihilation $XX \rightarrow J$, and therefore is not bounded by 1. We used Cirelli's data and associated Mathematica package [29], which greatly simplified our work.

Now that we are ready, consider an energy bin $[E_1, E_2]$. The conservative constraints on the number of photons in this bin N_c , as inferred from the cross-section constraints (σ_{WW} and $\sigma_{\tau\tau}$) on these channels, are:

$$N_{c,WW}(E_1, E_2) = \mathcal{L} \sigma_{WW} \int_{E_1}^{E_2} \frac{dn_{WW}}{dE} dE, \quad (\text{B.3})$$

$$N_{c,\tau\tau}(E_1, E_2) = \mathcal{L} \sigma_{\tau\tau} \int_{E_1}^{E_2} \frac{dn_{\tau\tau}}{dE} dE. \quad (\text{B.4})$$

Therefore, the conservative upper bound on the number of observed photons in this bin is:

$$N_c(E_1, E_2) = \max(N_{c,WW}(E_1, E_2), N_{c,\tau\tau}(E_1, E_2)). \quad (\text{B.5})$$

On the other hand, given the annihilation cross-section, $\sigma_{ann} = \sigma(XX \rightarrow H^\dagger H)$, we can compute the predicted number of photons in this bin:

$$N_p(E_1, E_2) = \mathcal{L} \int_{E_1}^{E_2} \frac{\sigma_{ann}}{4} \left(\frac{dn_{hh}}{dE} + 2 \frac{dn_{W_L W_L}}{dE} + \frac{dn_{Z_L Z_L}}{dE} \right) dE. \quad (\text{B.6})$$

Given that we want to constrain σ_{ann} , we require that,

$$N_p(E_1, E_2) \leq N_c(E_1, E_2), \quad (\text{B.7})$$

for all choices of (E_1, E_2) within the observational range of HESS: 10 GeV – 30 TeV. This means that the inequality in Eq. (B.7) has to be satisfied at the integrand level,

$$\frac{\sigma_{ann}}{4} \left(\frac{dn_{hh}}{dE} + 2 \frac{dn_{W_L W_L}}{dE} + \frac{dn_{Z_L Z_L}}{dE} \right) \leq \max \left(\sigma_{WW} \frac{dn_{WW}}{dE}, \sigma_{\tau\tau} \frac{dn_{\tau\tau}}{dE} \right), \quad \forall E \in [10\text{GeV}, 30\text{TeV}]. \quad (\text{B.8})$$

Finally, this implies that the bound on σ_{ann} is:

$$\sigma_{ann} \leq \min_{E \in [10\text{GeV}, 30\text{TeV}]} \left[\frac{4 \max \left(\sigma_{WW} \frac{dn_{WW}}{dE}, \sigma_{\tau\tau} \frac{dn_{\tau\tau}}{dE} \right)}{\left(\frac{dn_{hh}}{dE} + 2 \frac{dn_{W_L W_L}}{dE} + \frac{dn_{Z_L Z_L}}{dE} \right)} \right]. \quad (\text{B.9})$$

C More on the RG flow of quartic couplings

Our β -functions, β_{λ_i} , have the usual definitions,

$$\beta_{\lambda_i}(\lambda_H, \lambda_X, \lambda_{HX}) = \frac{d\lambda_i}{d \log \mu}, \quad (\text{C.1})$$

where $\lambda_i \in \{\lambda_H, \lambda_X, \lambda_{HX}\}$ and μ is some RG scale. Unsurprisingly, we see similarities with ϕ^4 theory, where $\beta(\lambda) = 3\lambda^2/16\pi^2$. Here, we specifically find,

$$\begin{aligned} \beta_{\lambda_H}(\lambda_H, \lambda_X, \lambda_{HX}) &\approx \frac{3}{96\pi^2} (36\lambda_H^2 + \lambda_{HX}^2) + \mathcal{O}(\lambda_i^3) \\ \beta_{\lambda_X}(\lambda_H, \lambda_X, \lambda_{HX}) &\approx \frac{3}{16\pi^2} (\lambda_X^2 + \lambda_{HX}^2) + \mathcal{O}(\lambda_i^3) \\ \beta_{\lambda_{HX}}(\lambda_H, \lambda_X, \lambda_{HX}) &\approx \frac{1}{16\pi^2} (6\lambda_H\lambda_{HX} + \lambda_X\lambda_{HX} + 4\lambda_{HX}^2) + \mathcal{O}(\lambda_i^3) \end{aligned} \quad (\text{C.2})$$

Note that the slightly differing pre-factors in the expressions above are merely an artefact of the way λ_H is normalised in the conventional SM, versus the more canonical way in which λ_X and λ_{HX} have been normalised.

As explained in Section 4.2, to ensure vacuum stability we require that λ_X does not become negative when RG running down from the Higgsplosion scale, E_H , to the DM mass, m_X . Above $\mu = E_H$, the RG flow is frozen by Higgsplosion. This is also the scale at which we require that $\lambda_X \ll \lambda_{HX}$ in order to prevent a significant contribution to m_X .

Suppose we set our new non-SM couplings at the Higgsplosion scale, $\mu = E_H = E_H(m_X)$, as follows,

$$\lambda_H(v_{EW}) = 1/8 \quad \lambda_X(E_H) = \hat{\lambda}_X \quad \lambda_{HX}(E_H) = 16\pi^2 \left(\frac{m_X}{E_H(m_X)} \right)^2, \quad (C.3)$$

where $\lambda_{HX}(E_H)$ is fully determined by our choice of DM mass, the relation in Eq. 2.9 and the requirement for correct relic abundance. For now, $\hat{\lambda}_X$ is left as a free parameter.

Any running derived from the β functions above is valid down to $\mu = m_X$. Hence, we now ask, how valid is our approximation, $\lambda_X \ll \lambda_{HX}$, if we demand vacuum stability? In other words, what is the lowest $\hat{\lambda}_X$ one can start with and not run into negative values for scales $m_X < \mu < E_H$? We focus on the two extremal non-excluded cases found in Section 3.5: $(m_X/\text{TeV}, \lambda_{HX}, E_H/\text{TeV}) = (0.7, 0.2, 19)$ and $(15, 5, 85)$.

For the lower DM mass bound, $m_X = 0.7$ TeV, we find $\lambda_X/\lambda_{HX} \approx 1.3 \times 10^{-2}$, while for the upper bound, $m_X = 15$ TeV, we find $\lambda_X/\lambda_{HX} \approx 0.17$. So we see that our assumption, $\lambda_X \ll \lambda_{HX}$, becomes less applicable as the portal coupling, λ_{HX} , increases. However, even at the largest coupling, one still finds a fairly minimal ratio of $\approx 17\%$. Therefore, we conclude that any contributions from the quartic X vertex are too small to change any phenomenological aspects of the model presented in this work: vacuum stability at all scales is certainly achievable.

References

- [1] V. C. Rubin and W. K. Ford, Jr., *Rotation of the Andromeda Nebula from a Spectroscopic Survey of Emission Regions*, *ApJ* **159** (Feb., 1970) 379.
- [2] Planck Collaboration, P. A. R. Ade, N. Aghanim, M. Arnaud, M. Ashdown, J. Aumont et al., *Planck 2015 results. XIII. Cosmological parameters*, *AAP* **594** (Sept., 2016) A13, [[1502.01589](#)].
- [3] S. Alam, M. Ata, S. Bailey, F. Beutler, D. Bizyaev, J. A. Blazek et al., *The clustering of galaxies in the completed SDSS-III Baryon Oscillation Spectroscopic Survey: cosmological analysis of the DR12 galaxy sample*, *MNRAS* **470** (Sept., 2017) 2617–2652, [[1607.03155](#)].
- [4] D. A. Buote, T. E. Jeltema, C. R. Canizares and G. P. Garmire, *Chandra Evidence of a Flattened, Triaxial Dark Matter Halo in the Elliptical Galaxy NGC 720*, *ApJ* **577** (Sept., 2002) 183–196, [[astro-ph/0205469](#)].
- [5] D. Clowe, A. Gonzalez and M. Markevitch, *Weak lensing mass reconstruction of the interacting cluster 1E0657-558: Direct evidence for the existence of dark matter*, *Astrophys. J.* **604** (2004) 596–603, [[astro-ph/0312273](#)].
- [6] M. Markevitch, A. H. Gonzalez, D. Clowe, A. Vikhlinin, L. David, W. Forman et al., *Direct constraints on the dark matter self-interaction cross-section from the merging galaxy cluster 1E0657-56*, *Astrophys. J.* **606** (2004) 819–824, [[astro-ph/0309303](#)].
- [7] J. McDonald, *Gauge singlet scalars as cold dark matter*, *Phys. Rev. D* **50** (Sep, 1994) 3637–3649.
- [8] C. Burgess, M. Pospelov and T. ter Veldhuis, *The minimal model of nonbaryonic dark matter: a singlet scalar*, *Nuclear Physics B* **619** (2001) 709 – 728.
- [9] N. Arkani-Hamed, D. P. Finkbeiner, T. R. Slatyer and N. Weiner, *A theory of dark matter*, *Phys. Rev. D* **79** (Jan, 2009) 015014.
- [10] J. M. Cline, K. Kainulainen, P. Scott and C. Weniger, *Update on scalar singlet dark matter*, *Phys. Rev. D* **88** (2013) 055025, [[1306.4710](#)].
- [11] M. Escudero, A. Berlin, D. Hooper and M.-X. Lin, *Toward (Finally!) Ruling Out Z and Higgs Mediated Dark Matter Models*, *JCAP* **1612** (2016) 029, [[1609.09079](#)].
- [12] V. V. Khoze and M. Spannowsky, *Higsplosion: Solving the Hierarchy Problem via rapid decays of heavy states into multiple Higgs bosons*, [[1704.03447](#)].
- [13] V. V. Khoze and M. Spannowsky, *Higsploding universe*, *Phys. Rev. D* **96** (2017) 075042, [[1707.01531](#)].
- [14] V. V. Khoze, J. Reiness, M. Spannowsky and P. Waite, *Precision measurements for the Higsploding Standard Model*, [[1709.08655](#)].
- [15] V. V. Khoze, *Multiparticle production in the large λ limit: Realising Higsplosion in a scalar QFT*, [[1705.04365](#)].
- [16] M. V. Libanov, V. A. Rubakov, D. T. Son and S. V. Troitsky, *Exponentiation of multiparticle amplitudes in scalar theories*, *Phys. Rev. D* **50** (1994) 7553–7569, [[hep-ph/9407381](#)].
- [17] A. S. Gorsky and M. B. Voloshin, *Nonperturbative production of multiboson states and quantum bubbles*, *Phys. Rev. D* **48** (1993) 3843–3851, [[hep-ph/9305219](#)].

- [18] D. T. Son, *Semiclassical approach for multiparticle production in scalar theories*, *Nucl. Phys.* **B477** (1996) 378–406, [[hep-ph/9505338](#)].
- [19] J. Jaeckel and V. V. Khoze, *Upper limit on the scale of new physics phenomena from rising cross sections in high multiplicity Higgs and vector boson events*, *Phys. Rev.* **D91** (2015) 093007, [[1411.5633](#)].
- [20] J. S. Gainer, *Measuring the Higgspllosion Yield: Counting Large Higgs Multiplicities at Colliders*, [1705.00737](#).
- [21] G. Panico and A. Wulzer, *The Composite Nambu-Goldstone Higgs*, *Lect. Notes Phys.* **913** (2016) pp.1–316, [[1506.01961](#)].
- [22] E. W. Kolb and M. S. Turner, *The Early Universe*, *Front. Phys.* **69** (1990) 1–547.
- [23] S. Dodelson, *Modern cosmology*. Academic Press, San Diego, CA, 2003.
- [24] J. L. Feng, M. Kaplinghat and H.-B. Yu, *Sommerfeld Enhancements for Thermal Relic Dark Matter*, *Phys. Rev.* **D82** (2010) 083525, [[1005.4678](#)].
- [25] LUX collaboration, D. S. Akerib et al., *Results from a search for dark matter in the complete LUX exposure*, *Phys. Rev. Lett.* **118** (2017) 021303, [[1608.07648](#)].
- [26] XENON collaboration, E. Aprile et al., *First Dark Matter Search Results from the XENON1T Experiment*, *Phys. Rev. Lett.* **119** (2017) 181301, [[1705.06655](#)].
- [27] B. J. Mount et al., *LUX-ZEPLIN (LZ) Technical Design Report*, [1703.09144](#).
- [28] H.E.S.S. collaboration, V. Lefranc and E. Moulin, *Dark matter search in the inner galactic center halo with H.E.S.S.*, in *Proceedings, 51st Rencontres de Moriond, Cosmology session: La Thuile, Italy, March 19-26, 2016*, pp. 149–152, 2016. [1608.08453](#).
- [29] M. Cirelli, G. Corcella, A. Hektor, G. Hutsi, M. Kadastik, P. Panci et al., *PPPC 4 DM ID: A Poor Particle Physicist Cookbook for Dark Matter Indirect Detection*, *JCAP* **1103** (2011) 051, [[1012.4515](#)].
- [30] FERMI-LAT, MAGIC collaboration, M. L. Ahnen et al., *Limits to dark matter annihilation cross-section from a combined analysis of MAGIC and Fermi-LAT observations of dwarf satellite galaxies*, *JCAP* **1602** (2016) 039, [[1601.06590](#)].
- [31] A. Geringer-Sameth and S. M. Koushiappas, *Exclusion of Canonical Weakly Interacting Massive Particles by Joint Analysis of Milky Way Dwarf Galaxies with Data from the Fermi Gamma-Ray Space Telescope*, *Physical Review Letters* **107** (Dec., 2011) 241303, [[1108.2914](#)].
- [32] FERMI-LAT collaboration, M. Ackermann et al., *Constraining Dark Matter Models from a Combined Analysis of Milky Way Satellites with the Fermi Large Area Telescope*, *Phys. Rev. Lett.* **107** (2011) 241302, [[1108.3546](#)].
- [33] Y.-L. S. Tsai, Q. Yuan and X. Huang, *A generic method to constrain the dark matter model parameters from Fermi observations of dwarf spheroids*, *JCAP* **1303** (2013) 018, [[1212.3990](#)].
- [34] PLANCK collaboration, P. A. R. Ade et al., *Planck 2015 results. XX. Constraints on inflation*, *Astron. Astrophys.* **594** (2016) A20, [[1502.02114](#)].
- [35] M. Kawasaki, K. Nakayama and T. Sekiguchi, *CMB Constraint on Dark Matter Annihilation after Planck 2015*, *Phys. Lett.* **B756** (2016) 212–215, [[1512.08015](#)].

- [36] V. Lefranc, E. Moulin, P. Panci and J. Silk, *Prospects for Annihilating Dark Matter in the inner Galactic halo by the Cherenkov Telescope Array*, *Phys. Rev.* **D91** (2015) 122003, [[1502.05064](#)].
- [37] N. Craig, H. K. Lou, M. McCullough and A. Thalappilil, *The Higgs Portal Above Threshold*, *JHEP* **02** (2016) 127, [[1412.0258](#)].
- [38] R. Huo, M. Kaplinghat, Z. Pan and H.-B. Yu, *Signatures of Self-Interacting Dark Matter in the Matter Power Spectrum and the CMB*, [1709.09717](#).
- [39] S. Tulin and H.-B. Yu, *Dark Matter Self-interactions and Small Scale Structure*, [1705.02358](#).
- [40] J. A. Casas, D. G. Cerdeo, J. M. Moreno and J. Quilis, *Reopening the Higgs portal for single scalar dark matter*, *JHEP* **05** (2017) 036, [[1701.08134](#)].